

Piezoelectricity in nominally centrosymmetric phases

O a A a 

The a and b axes are defined as $a = \sqrt{2}a_0$ and $b = a_0$, where a_0 is the lattice constant of the parent perovskite structure.

a. Ferroelastic domains within ferroelastic phases and ferroelastic local domains in the paraphase. The a and b axes are defined as $a = \sqrt{2}a_0$ and $b = a_0$, where a_0 is the lattice constant of the parent perovskite structure. The a and b axes are defined as $a = \sqrt{2}a_0$ and $b = a_0$, where a_0 is the lattice constant of the parent perovskite structure.

b. Ferroelectric-like local polar structures within the paraelectric phase. The a and b axes are defined as $a = \sqrt{2}a_0$ and $b = a_0$, where a_0 is the lattice constant of the parent perovskite structure. The a and b axes are defined as $a = \sqrt{2}a_0$ and $b = a_0$, where a_0 is the lattice constant of the parent perovskite structure.

Let us consider the a and b axes are defined as $a = \sqrt{2}a_0$ and $b = a_0$, where a_0 is the lattice constant of the parent perovskite structure. The a and b axes are defined as $a = \sqrt{2}a_0$ and $b = a_0$, where a_0 is the lattice constant of the parent perovskite structure.

Intrinsic versus extrinsic reasonings. An effective a and b axes are defined as $a = \sqrt{2}a_0$ and $b = a_0$, where a_0 is the lattice constant of the parent perovskite structure. The a and b axes are defined as $a = \sqrt{2}a_0$ and $b = a_0$, where a_0 is the lattice constant of the parent perovskite structure.

The a and b axes are defined as $a = \sqrt{2}a_0$ and $b = a_0$, where a_0 is the lattice constant of the parent perovskite structure. The a and b axes are defined as $a = \sqrt{2}a_0$ and $b = a_0$, where a_0 is the lattice constant of the parent perovskite structure.

The a and b axes are defined as $a = \sqrt{2}a_0$ and $b = a_0$, where a_0 is the lattice constant of the parent perovskite structure. The a and b axes are defined as $a = \sqrt{2}a_0$ and $b = a_0$, where a_0 is the lattice constant of the parent perovskite structure.

II. METHODS

Measurements were performed on single crystals of BaTiO_3 and BaTiO_3 doped with Ca , Ce , and La ions.

The a and b axes are defined as $a = \sqrt{2}a_0$ and $b = a_0$, where a_0 is the lattice constant of the parent perovskite structure.

TABLE I. Characteristics of the ferroelectric materials, T_c and T_f are defined as the Curie and the ferroelectric-paraelectric transition temperatures, respectively. Ref. [41–43].

Compound	Category	Curie Temperature (T_c)	Compound	Category	Ferroelectric Transition Temperature (T_f)
BaTiO ₃	Ferroelectric	$T_c = 401$ $T_c(\text{ceramic}) = 393$ K	0.6BaTiO ₃ -0.4 BaZrO ₃ (BZT40)	Relaxor	$T_f = 65$ K
LiTaO ₃	Ferroelectric	$T_c = 891$ K	LaAlO ₃	Ferroelastic	$T_c = 820$ K

FIG. 2. The piezoelectric coefficient d_{33} of the RPS and RUS, respectively.

B. How to extract the piezoelectric response from the spectra

In RPS, because of the piezoelectric effect, the piezoelectric coefficient d_{33} is related to the piezoelectric response d_{33} as follows:



FIG. 2. Piezoelectric characterization of LNbO₃ and PZT-5H. (a) Schematic of the piezoelectric device with a $d_{31} = 2.5$ pm/V coefficient. (b) Raman spectroscopy (RUS) plot showing intensity vs. frequency (kHz) with a peak at approximately 800 kHz. (c) Raman spectroscopy (RPS) plot showing intensity vs. frequency (kHz) with a peak at approximately 800 kHz. (d) Piezoelectric coefficient (d_{31}) vs. frequency (kHz) plot showing a peak at approximately 800 kHz. $V_{AC} = 10$ V.

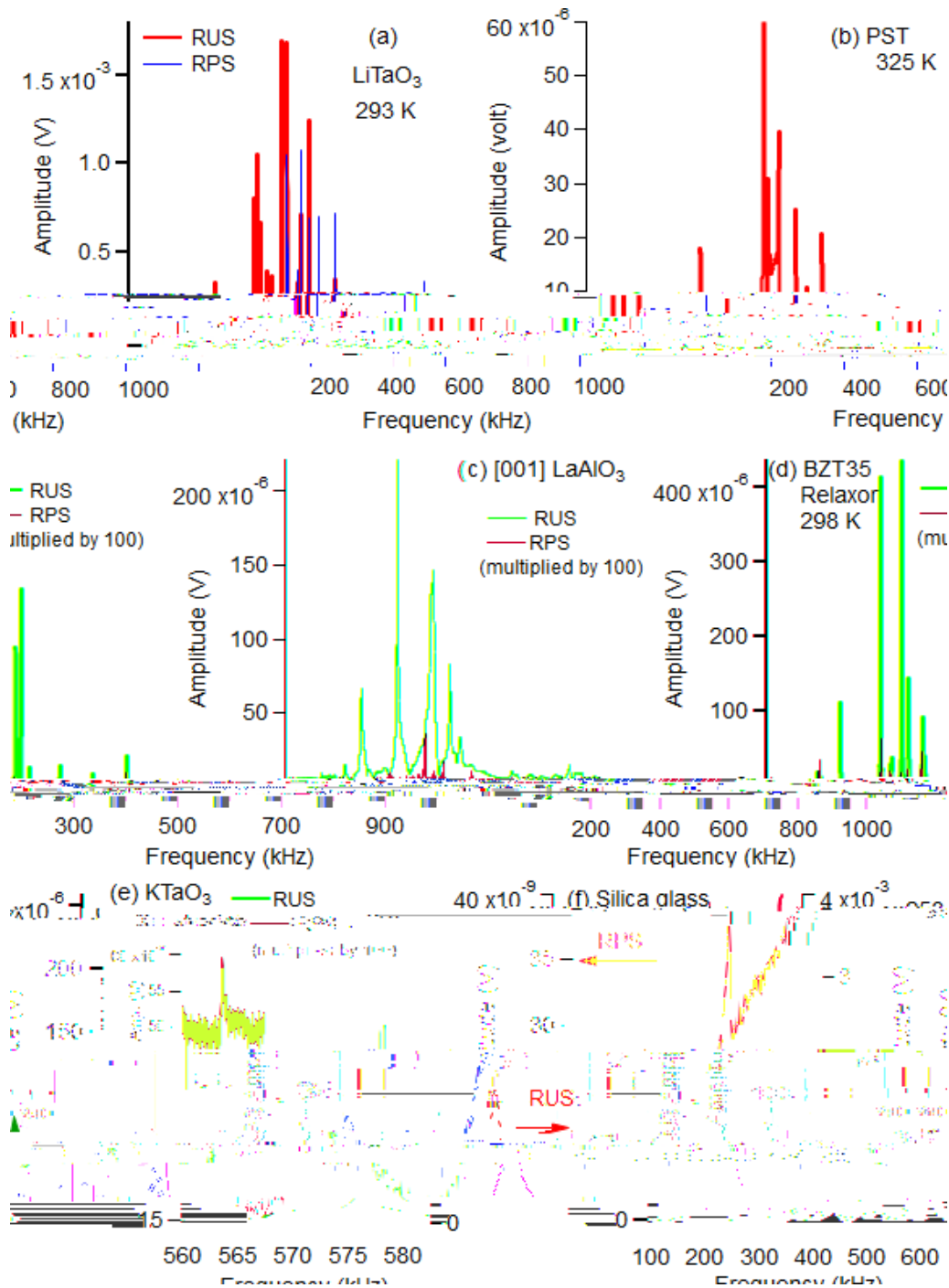


FIG. 4. Piezoelectric response spectra for various materials. (a) LiTaO_3 at 293 K, (b) PST at 325 K, (c) $[001] \text{LaAlO}_3$, (d) BZT35 Relaxor at 298 K, (e) KTaO_3 , and (f) Silica glass. RUS and RPS amplitudes are shown in Volts (V) versus Frequency (kHz). RUS amplitudes range from 10^{-3} to 10^{-8} V, and RPS amplitudes range from 10^{-3} to 10^{-8} V.

V. CURRENT UNDERSTANDING OF SPONTANEOUS ATOMIC-SCALE SYMMETRY BREAKING IN PARAPHASES

The piezoelectric response in paraphases is determined by the atomic-scale symmetry breaking. The piezoelectric response is a result of the spontaneous symmetry breaking in the paraphase region. The piezoelectric response is a result of the spontaneous symmetry breaking in the paraphase region. The piezoelectric response is a result of the spontaneous symmetry breaking in the paraphase region.

The piezoelectric response in paraphases is determined by the atomic-scale symmetry breaking. The piezoelectric response is a result of the spontaneous symmetry breaking in the paraphase region. The piezoelectric response is a result of the spontaneous symmetry breaking in the paraphase region. The piezoelectric response is a result of the spontaneous symmetry breaking in the paraphase region.

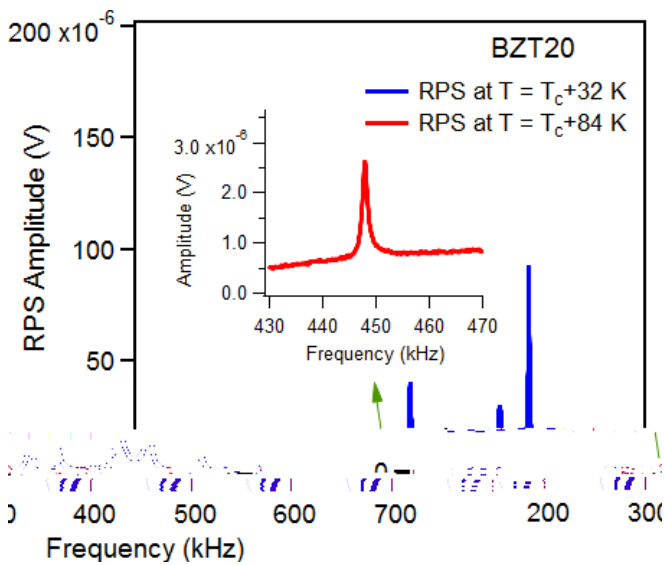


FIG. 5. Calculated RPS spectra for BZT20 at 32 and 84 K above the Curie temperature $T_c = 296$ K.

are calculated using the fast Fourier transform (FFT) method (MD) [80,83], and the average (S) of the calculated RPS spectra is shown in Fig. 5. The RPS spectra are calculated using the FFT method (MD) [80,83], and the average (S) of the calculated RPS spectra is shown in Fig. 5. The RPS spectra are calculated using the FFT method (MD) [80,83], and the average (S) of the calculated RPS spectra is shown in Fig. 5.

are calculated using the fast Fourier transform (FFT) method (MD) [80,83], and the average (S) of the calculated RPS spectra is shown in Fig. 5. The RPS spectra are calculated using the FFT method (MD) [80,83], and the average (S) of the calculated RPS spectra is shown in Fig. 5.

